J|A|C|S
ARTICLES
Published on Web 10/27/2006

Polyhedral Gold Nanocrystals with O_h Symmetry: From Octahedra to Cubes

Daeha Seo, Ji Chan Park, and Hyunjoon Song*

Contribution from the Department of Chemistry and School of Molecular Science (BK 21), Korea Advanced Institute of Science and Technology, Daejeon 305-701, Korea

Received April 26, 2006; Revised Manuscript Received August 30, 2006; E-mail: hsong@kaist.ac.kr

Abstract: We report the shape and size control of polyhedral gold nanocrystals by a modified polyol process. The rapid reduction of gold precursors in refluxing 1,5-pentanediol has successfully provided a series of gold nanocrystals in the shape of octahedra, truncated octahedra, cuboctahedra, cubes, and higher polygons by incremental changes of silver nitrate concentration. All nanocrystals were obtained quantitatively and were uniform in shape and size in the range of ~100 nm. Smaller octahedra and cubes were also prepared by using large amounts of PVP. Silver species generated from $AgNO_3$ seemed to determine the final nanocrystal morphology by the selective growth of {111} and/or the restriction of {100}. The shape evolution of the particles was addressed by quenching the reactions at different time intervals. The ~60 nm seeds were generated rapidly and grown slowly with simultaneous edge sharpening. Aging the reaction mixture focused the size and shape of the nanocrystals by Ostwald ripening. We believe that our selective growth conditions can be applied to other shapes and compositions of face-centered cubic metals.

1. Introduction

The control of metal nanostructure morphology (size, shape, and surface structure) has attracted much attention in recent years due to the interest in precise tuning of electronic, optical, and catalytic properties.[1] In particular, gold nanocrystals have been widely studied because of their high chemical and thermal stability, intense surface plasmon resonance scattering character, and ease in synthesis.[2] Spherical gold nanoparticles have been commonly employed as an electronic reservoir or a supporter for chemical and bio-functionality.[2,3] Since it has been reported that the UV absorption of gold nanorods can be carefully adjusted by changing their aspect ratio,[1d,4] a variety of gold nanostructures (rods,[4−6] plates,[7] branched structures,[8] and other forms[9]) have been prepared by different synthetic methods. However, the application of gold nanocrystals other than spherical particles is still rare, due to their small-scale production, extreme sensitivity, and poor reproducibility.

Although there were no reports of generalized synthetic routes and mechanisms reported thus far, some research groups have led pioneering efforts toward the rational control of metallic nanostructures, an ultimate goal in this field. Murphy et al. have reported a seed-mediated growth of gold nanorods with controllable aspect ratio of ~2 to ~25.[5] The reaction conditions of this method are mild (water, room temperature), and product formation can be scaled up to approximately one gram.[10] Tunable optical properties of nanorods led to their application in surface plasmon-based sensors and near-IR imaging.[11] Recently, Sau et al. have shown that multiple shapes of gold nanoparticles such as hexagons, cubes, and branched structures can be prepared in conditions almost analogous to those used in rod synthesis.[12]

Xia opens up the possibility of a general methodology for shape control in metallic nanostructures using the modified polyol process.[13] Metal chlorides and nitrates were used to make nanoparticles in polyol, mainly ethylene glycol (EG), in the

(1) (a) Xia, Y.; Halas, N. J. *Mater. Res. Soc. Bull.* **2005**, *30*, 338−348. (b) Murphy, C. J. *Science* **2002**, *298*, 2139−2140. (c) Kamat, P. V. *J. Phys. Chem. B* **2002**, *106*, 7729−7744. (d) El-Sayed, M. A. *Acc. Chem. Res.* **2001**, *34*, 257−264.
(2) (a) Daniel, M.-C.; Astruc, D. *Chem. Rev.* **2004**, *104*, 293−346. (b) Templeton, A. C.; Wuelfing, W. P.; Murray, R. W. *Acc. Chem. Res.* **2000**, *33*, 27−36.
(3) (a) Thomas, K. G.; Kamat, P. V. *Acc. Chem. Res.* **2003**, *36*, 888−898. (b) Quinn, B. M.; Liljeroth, P.; Ruiz, V.; Laaksonen, T.; Kontturi, K. *J. Am. Chem. Soc.* **2003**, *125*, 6644−6645. (c) Nam, J.-M.; Thaxton, C. S.; Mirkin, C. A. *Science* **2003**, *301*, 1884−1886. (d) Taton, T. A.; Mirkin, C. A.; Letsinger, R. L. *Science* **2000**, *289*, 1757−1760. (e) Elghanian, R.; Storhoff, J. J.; Mucic, R. C.; Letsinger, R. L.; Mirkin, C. A. *Science* **1997**, *277*, 1078−1081.
(4) (a) Link, S.; El-Sayed, M. A. *J. Phys. Chem. B* **1999**, *103*, 8410−8426. (b) Yu, Y.-Y.; Chang, S.-S.; Lee, C.-L.; Wang, C. R. C. *J. Phys. Chem. B* **1997**, *101*, 6661−6664.
(5) (a) Murphy, C. J.; Sau, T. K.; Gole, A. M.; Orendorff, C. J.; Gao, J.; Gou, L.; Hunyadi, S. E.; Li, T. *J. Phys. Chem. B* **2005**, *109*, 13857−13870. (b) Murphy, C. J.; Sau, T. K.; Gole, A.; Orendorff, C. J. *Mater. Res. Soc. Bull.* **2005**, *30*, 349−355. (c) Murphy, C. J.; Jana, N. R. *Adv. Mater.* **2002**, *14*, 80−82.
(6) Kim, F.; Song, J. H.; Yang, P. *J. Am. Chem. Soc.* **2002**, *124*, 14316−14317.
(7) (a) Ah, C. S.; Yun, Y. J.; Park, H. J.; Kim, W.-J.; Ha, D. H.; Yun, Y. S. *Chem. Mater.* **2005**, *17*, 5558−5561. (b) Wang, L.; Chen, X.; Zhan, J.; Chai, Y.; Yang, C.; Xu, L.; Zhuang, W.; Jing, B. *J. Phys. Chem. B* **2005**, *109*, 3189−3194. (c) Millston, J. E.; Park, S.; Shuford, K. L.; Qin, L.; Schatz, G. C.; Mirkin, C. A. *J. Am. Chem. Soc.* **2005**, *127*, 5312−5313.
(8) (a) Chen, S.; Wang, Z. L.; Ballato, J.; Foulger, S. H.; Carroll, D. L. *J. Am. Chem. Soc.* **2003**, *125*, 16186−16187. (b) Kuo, C.-H.; Huang, M. H. *Langmuir* **2005**, *21*, 2012−2016. (c) Hao, E.; Bailey, R. C.; Schatz, G. C.; Hupp, J. T.; Li, S. *Nano Lett.* **2004**, *4*, 327−330.
(9) (a) Chen, Y.; Gu, X.; Nie, C.-G.; Jiang, Z.-Y.; Xie, Z.-X.; Lin, C.-J. *Chem. Commun.* **2005**, 4181−4183. (b) Pei, L.; Mori, K.; Adach, M. *Langmuir* **2004**, *20*, 7837−7843. (c) Kuo, C.-H.; Chiang, T.-F.; Chen, L.-J.; Huang, M. H. *Langmuir* **2004**, *20*, 7820−7824.
(10) Jana, N. R. *Small* **2005**, *1*, 875−882.
(11) (a) Sönnichsen, C.; Alivisatos, P. *Nano Lett.* **2005**, *5*, 301−304. (b) Liao, H.; Hafner, J. H. *Chem. Mater.* **2005**, *17*, 4636−4641.
(12) Sau, T. K.; Murphy, C. J. *J. Am. Chem. Soc.* **2004**, *126*, 8648−8649.

presence of poly(vinyl pyrrolidone) (PVP). EG dissolves the metal salts and polar ligands in high concentrations and is able to allow the reaction mixture to surpass 190 °C. It also has enough reduction power for various metal ions; the reduction rates are carefully adjustable through the reaction temperature. After the reaction, EG is readily removed from the reaction media either by evaporation or by separation via decanting of the supernatant liquid after centrifugation. Such versatile features of EG enabled researchers to provide numerous noble metal nanostructures including silver,[13,14] palladium,[15] and platinum[16] nanoparticles and nanowires. They could further adjust the reduction rates of metal salts by addition of $FeCl_3$, $NaNO_3$, or HCl to afford novel shapes.[17] This method is now widely applicable to the synthesis of various metal, metal oxide, and semiconductor colloids under appropriate precursor/solvent pairs.[18]

Yang et al. have prepared isotropic gold nanostructures of truncated tetrahedra, cubes, and icosahedra termed "platonic nanocrystals" by a polyol process.[19] Importantly, these highly symmetric structures can provide fundamental insights into the origin of symmetry and formation mechanism of nanoscale materials. Herein, we use the modified polyol process for rational shape and size isotropic nanocrystal control. The use of 1,5-pentanediol (PD) as a solvent is very effective for the shape evolution of gold nanocrystals at high temperature. The final shapes, from octahedral to truncated octahedral, cuboctahedral, and cubic, have been synthesized quantitatively by using different amounts of $AgNO_3$, which may be attributed to the selective deposition of silver species on the seed surface during the reaction. Mechanistic aspects of gold nanocrystal shape formation are also discussed.

2. Experimental Section

Chemicals. Tetrachloroaurate trihydrate ($HAuCl_4 \cdot 3H_2O$, 99.9+%), silver nitrate ($AgNO_3$, 99+%), poly(vinyl pyrrolidone) (PVP, M_w = 55 000), and 1,5-pentanediol (PD, 96%) were purchased from Aldrich and used without further purification.

Synthesis of Polyhedral Gold Nanocrystals. 0.15 mL of $AgNO_3$ solution in PD was added to 5.0 mL of boiling PD. Next, 3.0 mL of PVP (0.15 M) and 3.0 mL of $HAuCl_4$ (0.050 M) PD solutions were alternatively added every 30 s over 7.5 min. The resulting mixture was refluxed for 1 h. The final solution was cooled, and the particles were separated from large aggregates by centrifugation at 500 rpm for 5 min. The product was purified by repetitive dispersion/precipitation cycle with ethanol to remove excess PVP, and finally dispersed in ethanol (30 mL) with the aid of sonication.

Different concentrations of $AgNO_3$ solution in PD were used for the syntheses of octahedra (1.7 mM, Ag/Au molar ratio = 1/600), truncated octahedra (2.0 mM, Ag/Au = 1/500), cuboctahedra (2.5 mM, Ag/Au = 1/400), cubes (5.0 mM, Ag/Au = 1/200), and higher polygons (17 mM, Ag/Au = 1/60).

For the smaller gold octahedra and cubes, 3.0 mL of PVP solution (1.0 M) in PD was added to the reaction mixture in the same concentration as the gold precursors.

Growth Mechanism Study. To address the size and shape change of the particles during the reaction, the reactions were quenched at 1, 3, 5, 7, and 15 min after the first addition of PVP and gold precursor solutions. The products were washed by repetitive dispersion/precipitation with ethanol. All samples were checked by scanning electron microscopy (SEM) and UV/vis absorption spectroscopy.

Characterization of Gold Nanocrystals. Transmission electron microscopy (TEM) and high-resolution TEM (HRTEM) images, and corresponding electron diffraction (ED) and energy-dispersive X-ray spectroscopy (EDX) patterns were obtained on a Tecnai F20 FE-TEM operated at 200 kV at KAIST and Korea Basic Science Institute (KBSI). SEM images were obtained using a Philips XL30S FEG operated at 10 and 3 kV. X-ray diffraction (XRD) patterns were measured on a Rigaku D/max-IIIC (3 kW) diffractometer using Cu Kα radiation. X-ray photoelectron spectroscopy (XPS) studies were carried out using a VG ESCA2000 with a Mg Kα source. The samples were prepared by placing a few drops of the colloidal solutions either on copper grids coated with lacey carbon film (Ted Pella, Inc.) for TEM, or on small pieces (5 mm × 5 mm) of silicon wafer (P-100) for SEM, XRD, and XPS, and were allowed to dry in air. Elemental analysis of the gold cubes was carried out by inductively coupled plasma (ICP) analysis using Spectro Ciros Vision at Korea Research Institute of Analytical Technology. The UV/vis absorption data were collected on a Jasco V530 UV/vis spectrophotometer using colloidal ethanol suspension. The IR spectrum was recorded on a Bruker EQUINOX 55 spectrometer.

3. Results

Synthesis of Polyhedral Gold Nanocrystals. Gold nanocrystals were synthesized by a modified polyol process,[13,19] which uses diol both as a solvent and as a reductant together in the presence of PVP, a surface regulating polymer. In the reaction procedure, PD solutions of tetracholoroaurate and PVP were added to the reaction mixture slowly. Different amounts of $AgNO_3$ solution were introduced to boiling PD prior to adding the reactants. The yellowish solution turned red immediately after the addition of gold precursors, and the final colloidal solution was reddish brown. Most particles were stable in ethanol for more than 1 week at room temperature, but precipitated during centrifugation at 6000 rpm for 30 min. Repetitive precipitation/dispersion can purify gold nanocrystals from the mixture of unreacted metal precursors and excess PVP.

All nanocrystals synthesized under the different conditions were analyzed via SEM and TEM. Gold clumps larger than the micrometer range were generated by the addition of gold precursors and PVP without additives. Yet, when a small amount of $AgNO_3$ (1/600 equiv with respect to the gold concentration) was introduced, the product particles became uniformly octahedral. Figure 1 shows representative images of gold octahedra. The particles are aligned along their C_3 axes normal to the surface; thus a two-dimensional particle projection gives a regular hexagon. The C_4 symmetric structures are also shown in Figure 1c, indicative of ideal O_h nanocrystal symmetry. The average edge length is approximately 100 nm with a distribution of $\sigma = \sim 10\%$ (Figure S1, Supporting Information). The ED pattern of a single particle (Figure 1f, inset) indicates that the particle is a single crystal with the zone axis of ⟨111⟩ and exposed surface of {111} face.

(13) (a) Wiley, B.; Sun, Y.; Mayers, B.; Xia, Y. *Chem. Eur. J.* **2005**, *11*, 454−463. (b) Wiley, B.; Sun, Y.; Chen, J.; Cang, H.; Li, Z.-Y.; Li, X.; Xia, Y. *Mater. Res. Soc. Bull.* **2005**, *30*, 356−361.
(14) (a) Sun, Y.; Xia, Y. *Science* **2002**, *298*, 2176−2179. (b) Wiley, B.; Herricks, T.; Sun, Y.; Xia, Y. *Nano Lett.* **2004**, *4*, 1733−1739. (c) Sun, Y.; Yin, Y.; Mayers, B. T.; Herricks, T.; Xia, Y. *Chem. Mater.* **2002**, *14*, 4736−4745.
(15) Xiong, Y.; Chen, J.; Wiley, B.; Xia, Y. *J. Am. Chem. Soc.* **2005**, *127*, 7332−7333.
(16) (a) Chen, J.; Herricks, T.; Xia, Y. *Angew. Chem., Int. Ed.* **2005**, *44*, 2589−2592. (b) Chen, J.; Herricks, T.; Geissler, M.; Xia, Y. *J. Am. Chem. Soc.* **2004**, *126*, 10854−10855.
(17) (a) Wiley, B.; Sun, Y.; Xia, Y. *Langmuir* **2005**, *21*, 8077−8080. (b) Herricks, T.; Chen, J.; Xia, Y. *Nano Lett.* **2004**, *4*, 2367−2371. (c) Im, S. H.; Lee, Y. T.; Wiley, B.; Xia, Y. *Angew. Chem., Int. Ed.* **2005**, *44*, 2154−2157.
(18) (a) Wang, Y.; Xia, Y. *Adv. Mater.* **2005**, *17*, 473−477. (b) Wang, Y.; Xia, Y. *Nano Lett.* **2004**, *4*, 2047−2050. (c) Wang, Y.; Jiang, X.; Xia, Y. *J. Am. Chem. Soc.* **2003**, *125*, 16176−16177.
(19) Kim, F.; Connor, S.; Song, H.; Kuykendall, T.; Yang, P. *Angew. Chem., Int. Ed.* **2004**, *43*, 3673−3677.

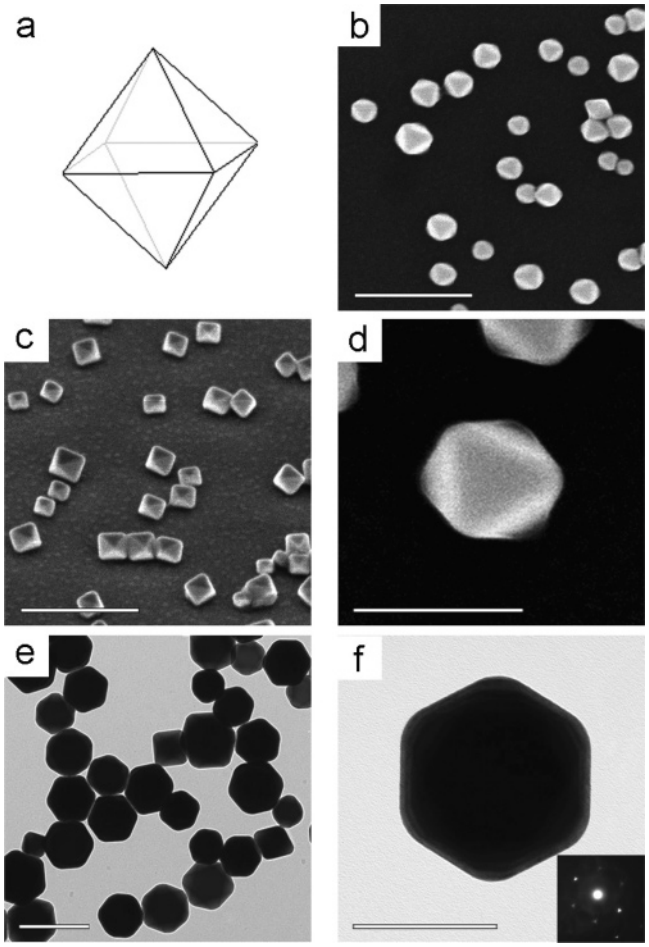

Figure 1. Gold octahedron nanocrystals. (a) Ideal octahedron structure. (b−d) SEM images of the octahedra in a view normal to the substrate (b,d) and tilted 45° (c). (e,f) TEM images of the octahedra. Inset in (f) is an ED pattern. The bars indicate 500 nm (b,c), 200 nm (d,e), and 100 nm (f).

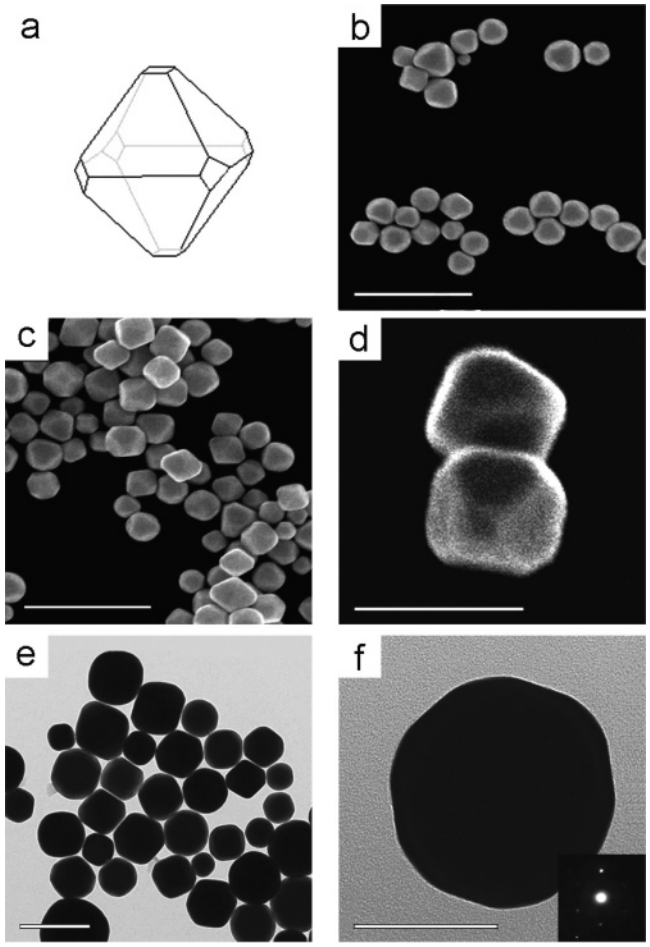

Figure 2. Gold truncated octahedron nanocrystals. (a) Truncated octahedron structure. (b−d) SEM images of the truncated octahedra in a view normal to the substrate (b,c) and with a 45° tilt (d). (e,f) TEM images of the truncated octahedra. Inset in (f) is an ED pattern. The bars indicate 500 nm (b,c), 200 nm (d,e), and 100 nm (f).

The use of 1/500 equiv $AgNO_3$ with respect to the gold precursor led to the truncation of the octahedral vertexes. Figure 2 exhibits nearly octahedron fashion of the nanocrystals with rounded apexes. The expanded image of a single crystal (Figure 2d) obviously represents truncated corners from the ideal octahedron structure. However, most of the exposed surface is still covered with {111} faces, so the ED pattern of the nanocrystal (Figure 2f inset) is hexagonal as similarly observed in the octahedron. The average edge length is 98 ± 13 nm, decreased from that of the octahedron due to truncation.

Higher concentrations of $AgNO_3$ (Ag/Au = 1/400) in the separate reaction batch provided more truncation of the edges affording cuboctahedra as seen in Figure 3. In the ideal cuboctahedron structure, the surface is covered with both {100} and {111} faces in an area ratio of 1:0.58. Therefore, the particles are likely to align along both the ⟨100⟩ and the ⟨111⟩ directions normal to the substrate, and a mixture of squares and hexagons appears in the TEM image (Figure 3d). EDs of the square and hexagonal projections show corresponding cubic and hexagonal patterns, respectively (Figure 3e and f).

Fully developed gold cubes were synthesized by the addition of 1/200 equiv of $AgNO_3$ to the reaction mixture. The particle has sharp edges and is uniformly shaped. The TEM image of a single crystal in Figure 4f reveals a perfect square with the electron diffraction pattern of {100} along the ⟨100⟩ zone axis. The average edge length is 145 ± 18 nm, as shown in Figure S1 of the Supporting Information.

When more $AgNO_3$ (Ag/Au = 1/60) was used in the reaction, nearly spherical particles were obtained. The surface of the particles comprises many different crystal faces, and the TEM image (Figure 5c) shows a polygonal structure. The particles are monodisperse with the average diameter of 77 ± 5.0 nm.

Characterization of Gold Nanocrystals. In XRD data, gold single crystal in a bulk substrate exhibits the typical diffraction patterns of face-centered cubic lattice, {111}, {200}, and {220}, with the relative intensities of 1:0.5:0.3, respectively. The gold polygon shows diffraction intensity ratios similar to the conventional ones. However, only a {111} peak appeared in the XRD spectrum for the gold octahedra, because of a preferential orientation of the particles along {111} planes parallel to the substrate. Gold nanocubes tend to orient along {100} planes on the substrate, making an exclusively high intensity of {200} signal.[17c] The diffraction pattern of the truncated octahedra is more like that for the octahedra, and the cuboctahedra have a higher intensity of {200} peak than that of {111}, as observed in Figure 6. These clear XRD patterns for each structure also confirm the high shape uniformity of the nanocrystals.

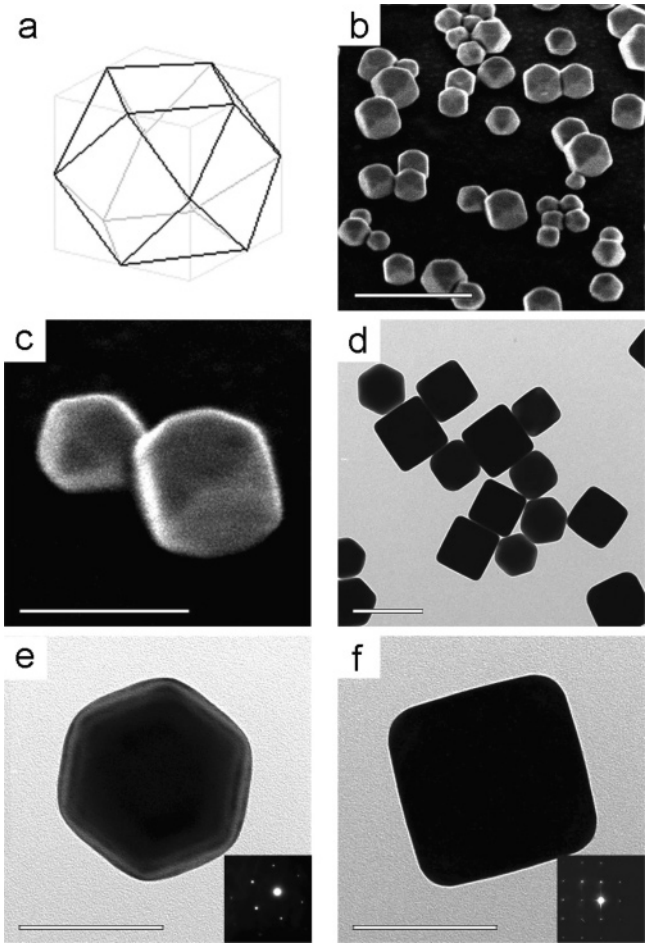

Figure 3. Gold cuboctahedron nanocrystals. (a) Ideal cuboctahedron structure. (b,c) SEM images of the cuboctahedra tilted 45° to the substrate. (d−f) TEM images of the cuboctahedra. Insets (e,f) are corresponding ED patterns. The bars indicate 500 nm (b), 200 nm (c,d), and 100 nm (e,f).

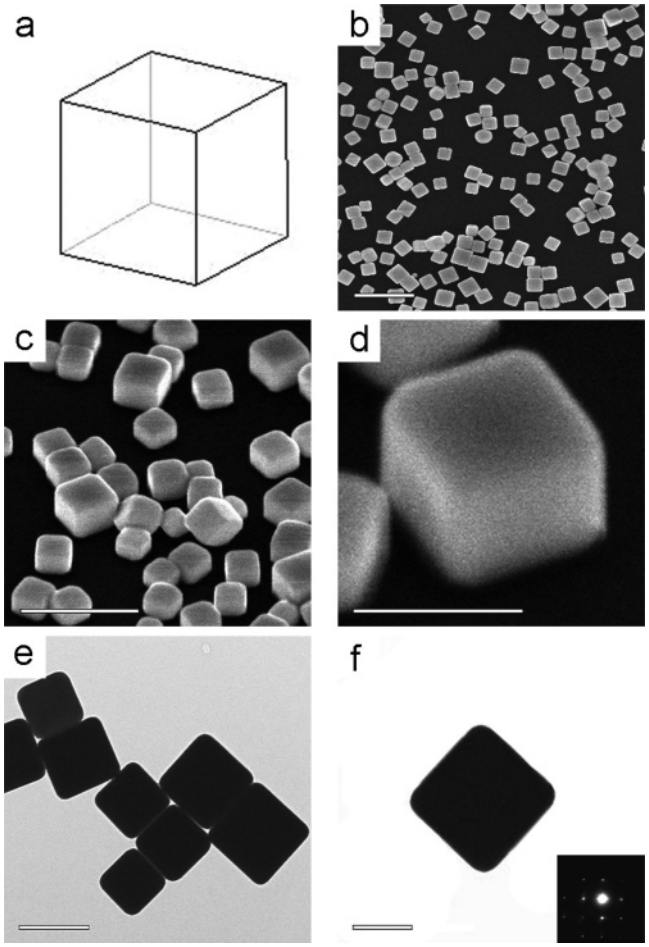

Figure 4. Gold cube nanocrystals. (a) Ideal cube structure. (b−d) SEM images of the cubes in a view normal to the substrate (b) and tilted 45° (c,d). (e,f) TEM images of the cubes. Inset in (f) is an ED pattern. The bars indicate 500 nm (b,c), 200 nm (d,e), and 100 nm (f).

Surface composition of the gold cubes was analyzed by XPS, revealing intense Ag($3d_{3/2}$) and Ag($3d_{5/2}$) bands as well as Au($4f_{5/2}$), Au($4f_{7/2}$), Au($4d_{3/2}$), Au($4d_{5/2}$), O(1s), C(1s), and Cl(2p) peaks (Figure 7a). The relative intensity of the silver bands corrected by a conversion factor is 11 mol % as compared to that of gold, although the elemental analysis for silver was only 0.9 mol % with respect to the gold content (Au 56.3 wt %; Ag 0.28 wt % by total weight of the gold cube sample). Such a large increment of the silver fraction in XPS reveals the silver residues are distributed mainly on the surface of the gold cubes, considering that the emitted electrons in XPS come from surface atoms in the range of 0.4−2.0 nm underneath a metallic surface.[20] Precise measurement of the silver peaks provides information of Ag species on the surface (Figure 7b). Deconvolution of the Ag($3d_{5/2}$) band gives three distinct peaks at 368.4, 367.7, and 361.0 eV, assignable to Ag, AgCl, and Ag_2CO_3, respectively, in which AgCl is the major component (~60% of the total Ag intensity). The O(1s) and N(1s) bands are mainly from the PVP moiety adsorbed on the gold cube surface (Figure S2, Supporting Information).

Gold nanocrystals normally show very intense color due to surface plasmon resonance scattering, which is highly dependent upon particle size and shape.[1a,21] The UV/vis absorption spectrum of the octahedra in ethanol shows a relatively sharp peak at 592 nm, whereas the truncated octahedra and cuboctahedra display a broad band at 579 nm (Figure 8). Two broad peaks at 593 and 669 nm are distinguishable for the cube structure. UV/vis absorption of the higher polygons is shifted to 542 nm, analogous to the absorption bands of smaller spherical particles made by seed-mediated growth.[22]

Synthesis of Smaller Nanocrystals. For controlling nanocrystal structure, the amounts of PVP in the reactions were fixed to 3 equiv with respect to gold concentration. Yet, when 20 equiv of PVP was used for the octahedra synthesis, smaller octahedra were obtained almost quantitatively. The average edge length of the product was estimated as 65 ± 7.8 nm by SEM, which is ca. 65% of the original edge length for the octahedra. The nanocrystals maintain nearly ideal octahedral geometry having C_3 and C_4 symmetry as shown in Figure 9a and b, and show single crystalline nature in ED pattern (Figure 9c, inset).

Smaller cubes can also be synthesized by adding 20 equiv of PVP. Figure 9d reveals gold cube structure with an average

(20) Somorjai, G. A. *Chemistry in Two Dimensions: Surfaces*; Cornell University Press: Ithaca, NY, 1981.

(21) (a) Hutter, E.; Fendler, J. H. *Adv. Mater.* **2004**, *16*, 1685−1706. (b) Kelly, K. L.; Coronado, E.; Zhao, L. L.; Schatz, G. C. *J. Phys. Chem. B* **2003**, *107*, 668−677. (c) Mock, J. J.; Barbic, M.; Smith, D. R.; Schultz, D. A.; Schultz, S. *J. Chem. Phys.* **2002**, *116*, 6755−6759.

(22) (a) Jana, N. R.; Gearheart, L.; Murphy, C. J. *Chem. Mater.* **2001**, *13*, 2313−2322. (b) Brown, K. R.; Walter, D. G.; Natan, M. J. *Chem. Mater.* **2000**, *12*, 306−313.

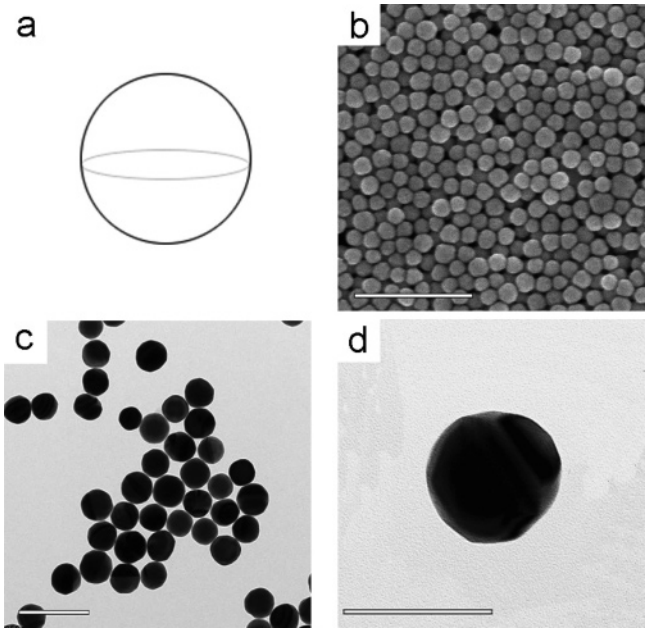

Figure 5. Gold higher polygon nanocrystals. (a) Ideal spherical structure. (b) SEM image of the higher polygons. (c,d) TEM images of the higher polygons. The bars indicate 500 nm in (b), 200 nm in (c), and 100 nm in (d).

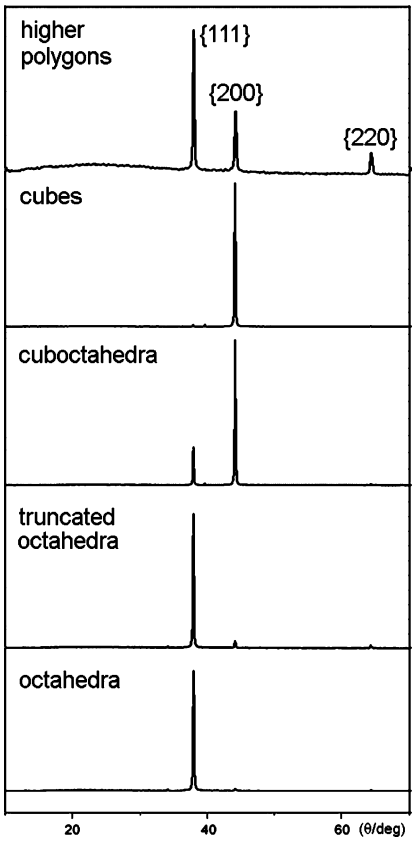

Figure 6. XRD spectra of polyhedral gold structures from octahedra to higher polygons.

edge of 80 ± 16 nm, 60% of the original cubes under the standard condition. The ED pattern of a smaller cube reveals an ideal cube structure (Figure 9f, inset). XRD data of the smaller nanostructures show only a {111} peak for the octahedra and a {200} peak for the cubes, respectively, similar to their larger counterparts.

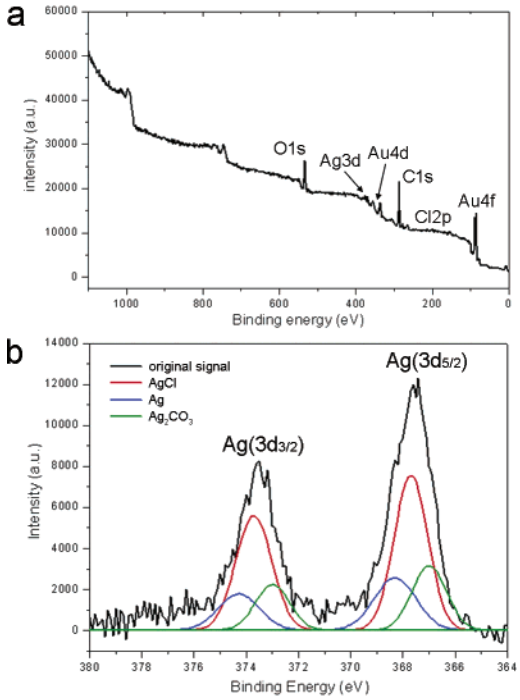

Figure 7. XPS spectra of the gold cubes (a) from a survey scan and (b) from the Ag(3d) energy region.

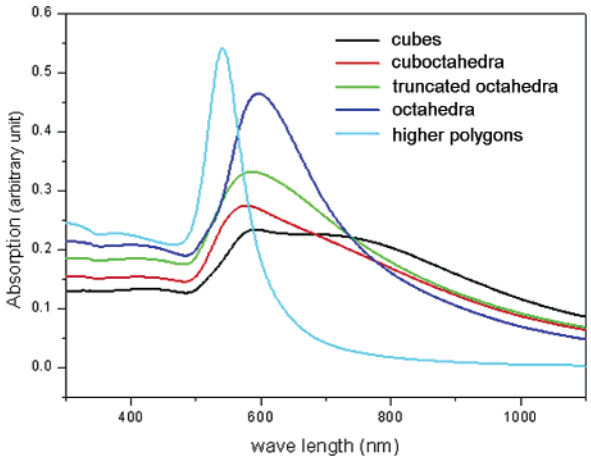

Figure 8. UV/vis spectra of the various nanocrystal shapes.

Structural Changes during the Reaction. During the cube synthesis, the reactions were quenched at various time intervals after the addition of the reactants to address the mechanism(s) related to crystal growth and shape formation. As soon as the gold precursors were added to boiling solvent, ~60 nm sized gold nanoparticles were formed rapidly (Figure 10a), which then grew to afford structures with more facets (Figure 10b). As the reaction went on, the edges of larger particles sharpened to afford crude cubes, while small particles were still being generated from gold precursors (Figure 10c and d). Even in the same batch, larger particles had sharper edges than did the smaller ones. Aging the reaction mixture allowed for the formation of regular structure, perfect cubes (Figure 10f). The average size distribution became broad during the addition of the reactants, but later narrowed giving uniform cubes with an edge length of ~140 nm after aging. The growth patterns for octahedra synthesis were also monitored this way, and the reaction progress was almost analogous to that of cube formation.

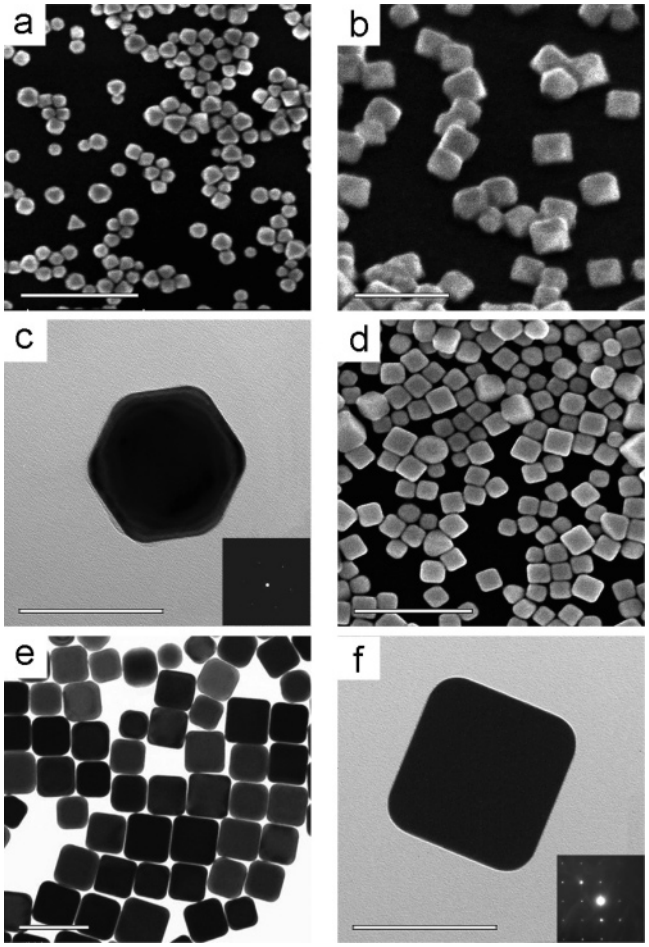

Figure 9. Smaller gold nanocrystals. SEM (a,b) and TEM (c) images of the smaller octahedra. SEM (d) and TEM (e,f) images of the smaller cubes. Insets in (c) and (f) are corresponding ED patterns. The bars indicate 500 nm (a,d), 200 nm (b,e), and 100 nm (c,f).

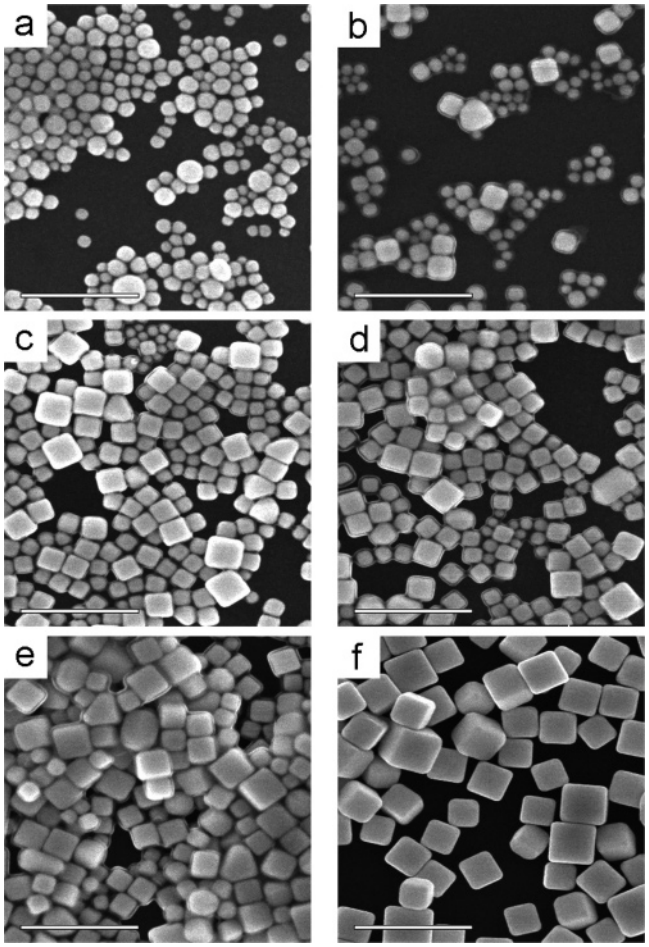

Figure 10. Mechanistic study of the gold cubes. SEM images of the gold nanocrystals sampled at (a) 1 min, (b) 3 min, (c) 5 min, (d) 7 min, (e) 15 min, and (f) 60 min after the first addition of gold precursor, respectively. The bars represent 500 nm.

4. Discussion

The Role of Reaction Media Components. For the rapid reduction of the gold precursor, all reactions were carried out in boiling PD, which is higher boiling (242 °C) than ethylene glycol (197 °C) and of sufficient solubility for dissolving gold precursors and PVP. The higher reaction temperature increases the formation of thermodynamically more stable structures, resulting in more uniform single-crystalline products, and reduces the formation of less stable twinned particles such as decahedra and rods. Xia et al. represented the selective removal of twinned particles under oxidative conditions, to gain single-crystal silver[14b] and palladium[15] particles in high yields. The main reaction may also be simplified and easily controlled at high temperature, because the reduction of gold precursor is a multistep process from Au(III) to Au(I) and eventually to Au(0) with the corresponding oxidation of PD and PVP. High temperature speeds up the forward reaction making gold nanocrystals, and thus various gold intermediates generated during the reaction do not affect the final product morphology. Experimentally, the gold nanocrystals with definite polyhedral shape were obtained almost exclusively in refluxing PD, but the gold precursors remained in the solution at lower temperatures even after sufficient heating of the reaction media, and the final product contained a large fraction of gold spheres, facets, and rods as well as single crystalline particles.

PVP is known to make nanoparticles stable in solution by strong binding to various silver nanostructure surfaces.[13,14] However, under our experimental conditions, PVP alone without $AgNO_3$ addition was not enough to stabilize the gold particles in solution. The introduction of $AgNO_3$ may suppress the growth of a certain face at some rates (vide infra), preventing a large cluster formation and rendering the nanocrystals stable. Interestingly, the increase of PVP concentration up to 20 equiv with respect to the gold concentration adjusts the nanocrystal size but still preserves the shape. It is presumably due to the nonselective PVP binding to the gold seed surface and the resulting restriction of crystal growth along all directions.

Mechanistic Aspects of the Formation of Polyhedral Gold Nanocrystals. The $AgNO_3$ concentration added to the reaction mixture greatly influences the shape and surface structure of the nanocrystals. The nanocrystal shape changed from octahedral to truncated octahedral, cuboctahedral, cubic, and spherical by incremental changes of $AgNO_3$ concentration in each reaction (Scheme 1). In terms of the surface structure, an octahedron has only {111} faces exposed to the surface, and {100} surface fraction continuously increases up to the cube with complete {100} coverage, as the $AgNO_3$ amount increases. It reveals that Ag species generated from $AgNO_3$ enhance the selective growth of {111} and/or suppress the growth of {100}. Similar

Scheme 1. Polyhedral Structures of Gold Nanocrystals with Respect to the $AgNO_3$ Amount Added in the Reaction Mixture

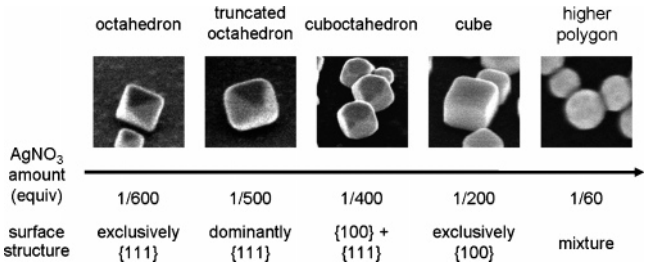

phenomena with silver ions were already observed in gold nanorods prepared by electrochemical,[4] seeding,[5] and photochemical methods.[6]

XPS analysis of the gold cubes indicates that the silver species participate in the redox reaction of the gold precursors that occurred on the seed surface. AgCl is formed from Ag^+ in the presence of chloride ions. AgCl is readily reduced to Ag(0) in PD at high temperature, and Ag(0) is oxidized again to Ag^+ and AgCl by a galvanic exchange reaction with $AuCl_4^-$, which is continuously added to the reaction mixture. Therefore, all three components, AgCl, Ag, and Ag^+, could be detected by XPS analysis. AgCl is the major species, presumably resulting from the precipitation of AgCl as a solid layer on the gold surface due to its low solubility in PD even at high temperature. These silver species play a crucial role in the shape control of nanocrystals. In a face-centered cubic lattice, {111} has the lowest energy. Yang et al. have demonstrated that truncated tetrahedra and icosahedra were predominantly obtained under the conditions without silver salts, in which the surfaces are covered with only {111} faces.[19] The octahedra with {111} surfaces were also synthesized at very low Ag^+ concentrations (1/1000−1/600 equiv with respect to the gold precursors) in our experiments. Yet, as the silver concentration increases, the {100} faces tend to increase on the surface because the silver species may be selectively bound to {100} and restrict the surface growth. Lorenz et al. have reported that in the underpotential deposition (UPD), silver is preferentially grown on Au(100), but not on Au(111) at the intermediate deposition rates.[23] Guyot-Sionnest et al. have elucidated the seed-mediated growth of gold nanorods and bipyramids by the selective UPD of silver ion on the gold surface.[24] Accordingly, the silver-to-gold ratio in the reaction mixture determines the relative growth rate of {100} as compared to that of {111}, leading to the final shape and morphology of the gold nanocrystals.[25] If the silver concentration is very high and exceeds the selective deposition condition, seed growth is completely restricted along all directions, leading to smaller spherical particles (higher polygons) as observed.

The progress of gold nanocube formation was addressed by quenching the reaction at different time intervals. The spherical seeds with a diameter of ~60 nm were immediately formed after the first addition of gold precursors and grew slowly into larger particles. Particle edge sharpening occurred concomitantly with particle growth. After the precursor addition was completed, aging the reaction mixture for 1 h provided uniform gold cubes with a narrow size distribution. At this stage, smaller seeds were dissolved again and larger particles grew more, which is typical of Ostwald ripening.[26] The total process is depicted in Scheme 2, summarized as rapid seed formation, edge sharpening, and shape and size focusing by Ostwald ripening subsequently.

Scheme 2. Proposed Formation of the Gold Nanocubes

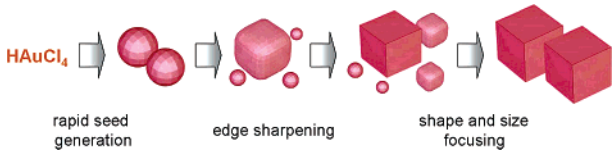

The octahedra synthesis follows a similar process, in which the seeds were rapidly formed and grew with simultaneous edge sharpening. It is worth noting that the size and shape of the higher polygons, prepared at a high $AgNO_3$ concentration, are comparable to the seed structure. It indicates that particle growth is completely restricted by the large amount of silver species during seed formation.

The selective adsorption of PVP on a certain surface structure is known to guide the crystal morphology in many cases.[6,13−18] The final gold crystals in our experiments also have a significant amount of PVP layers adsorbed on their surface, which can be analyzed by XPS and IR (Figure S2, Supporting Information). However, the contribution of PVP in the exclusive shape control seems to be limited and less than that of $AgNO_3$, because the small amount of PVP used in the reaction without $AgNO_3$ could not sufficiently stabilize the gold product. The use of a large amount of PVP (20 equiv) did not affect particle shape, but led to only a change in particle size.

5. Conclusion

Polyhedral gold nanocrystals with O_h symmetry were rationally synthesized by a modified polyol process in refluxing PD. Importantly, a wide range of O_h symmetric polyhedra (shapes ranging from the octahedron to the truncated octahedron, as well as the cuboctahedron, and cube) were able to be rationally and reproducibly prepared. The $AgNO_3$ concentration added in the reaction mixture plays a key role for structural fine-tuning. The smaller particles were obtained by using larger PVP amounts. The silver species generated from $AgNO_3$ appear to selectively suppress {100} surface growth and/or enhance {111} growth. The shape of the nanocrystals evolved sequentially through rapid seed formation, edge sharpening, and shape and size focusing by Ostwald ripening.

If the growth rates of {100} and {111} faces are precisely controllable, any particular shapes in a face-centered cubic lattice are attainable in the nanometer range. Our selective growth conditions may be extended to the synthesis of anisotropic nanocrystals such as rods, wires, and branched structures, which exhibit intriguing optical properties for biomedical applications.[11] We are also interested in the packing of polyhedral nanostructures into two- and three-dimensional architectures and their applications.

Acknowledgment. This work was supported by the Korean Research Foundation Grant funded by the Korean Government (MOEHRD) (KRF-2005-205-C00040). We thank Prof. Peidong Yang of the University of California, Berkeley, for helpful

(23) (a) Giménez, M. C.; Del Pópolo, M. G.; Leiva, E. P. M.; García, S. G.; Salinas, D. R.; Mayer, C. E.; Lorenz, W. J. *J. Electrochem. Soc.* **2002**, *149*, E109-E116. (b) Garcia, S.; Salinas, D.; Mayer, C.; Schmidt, E.; Staikov, G.; Lorenz, W. J. *Electrochim. Acta* **1998**, *43*, 3007−3019.
(24) Liu, M.; Guyot-Sionnest, P. *J. Phys. Chem. B* **2005**, *109*, 22192−22200.
(25) Wang, Z. L. *J. Phys. Chem. B* **2000**, *104*, 1153−1175.
(26) Hoang, T. K. N.; Deriemaeker, L.; La, V. B.; Finsy, R. *Langmuir* **2004**, *20*, 8966−8969 and references therein.

discussions. Prof. David G. Churchill of KAIST is acknowledged for his help in proofreading this manuscript.

Supporting Information Available: Low-resolution SEM image and analysis of particle size distribution for each nanocrystal shape, and XPS and IR data of the gold cubes. This material is available free of charge via the Internet at http://pubs.acs.org.

JA062892U